Asymmetric CorA Gating Mechanism as Observed by Molecular Dynamics Simulations

Nemchinova, Mariia; Melcr, Josef; Wassenaar, Tsjerk; Marrink, Siewert; Guskov, Albert

IMPORTANT NOTE: You are advised to consult the publisher's version (publisher's PDF) if you wish to cite from it. Please check the document version below.

Document Version
Version created as part of publication process; publisher's layout; not normally made publicly available

[Link to publication in University of Groningen/UMCG research database](#)

Article

Asymmetric CorA Gating Mechanism as Observed by Molecular Dynamics Simulations

Mariia Nemchinova, Josef Melcr, Tsjerk A. Wassenaar, Siewert J. Marrink,* and Albert Guskov*

Cite This: https://doi.org/10.1021/acs.jcim.1c00261

Read Online

ACCESS | 📊 Metrics & More | 📖 Article Recommendations | 🔘 Supporting Information

ABSTRACT: The CorA family of proteins plays a housekeeping role in the homeostasis of divalent metal ions in many bacteria and archaea as well as in mitochondria of eukaryotes, rendering it an important target to study the mechanisms of divalent transport and regulation across different life domains. Despite numerous studies, the mechanistic details of the channel gating and the transport of the metal ions are still not entirely understood. Here, we use all-atom and coarse-grained molecular dynamics simulations combined with *in vitro* experiments to investigate the influence of divalent cations on the function of CorA. Simulations reveal pronounced asymmetric movements of monomers that enable the rotation of the $\alpha 7$ helix and the cytoplasmic subdomain with the subsequent formation of new interactions and the opening of the channel. These computational results are functionally validated using site-directed mutagenesis of the intracellular cytoplasmic domain residues and biochemical assays. The obtained results infer a complex network of interactions altering the structure of CorA to allow gating. Furthermore, we attempt to reconcile the existing gating hypotheses for CorA to conclude the mechanism of transport of divalent cations via these proteins.
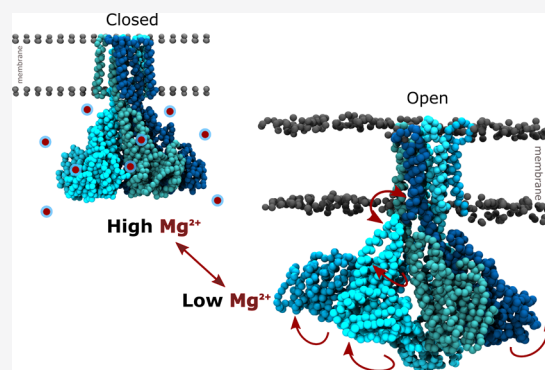
INTRODUCTION

The family of CorA membrane proteins is one of the most ancient transport systems for magnesium (and related divalent cations), conserved from bacteria to human mitochondria. A peculiarity is that these proteins transport hydrated cations but use a so-called hydrophobic gating mechanism[1]—where the transition from an anhydrous nonconductive state (closed state) to a functionally active state (open state) allows the flow of ions down the gradient.

To date, the most characterized among the CorA family of proteins is the one from the thermophilic bacterium *Thermotoga maritima* (TmCorA), which is an important model system for studying the divalent metal-ion transport via prokaryotic channels and their eukaryotic homologues.[2] *In vivo* as well as *in vitro* experimental studies of ion conductivity and transport showed that members of the family are capable of transporting several (but similar) divalent cations, including Mg^{2+}, Co^{2+}, Ni^{2+}, Zn^{2+}, and Cd^{2+}.[2−4]

Crystal structures of TmCorA, obtained in the presence of divalent cations,[5−8] revealed a pentameric assembly with a five-fold symmetry in the closed state, where long $\alpha 7$ helices twist into a left-handed helix, creating an ion pore (Figure 1). The C-terminal part is assembled by combining the end of an $\alpha 7$ helix (forming the transmembrane segment TM1), the periplasmic loop, which contains the signature motif glycine—methionine—asparagine (GMN) responsible for the selectivity of divalent cations, the MPEL motif loop (which is not present in many homologues), and the outer transmembrane helix (TM2) with

the KKKKWL motif at the end. The large N-terminal cytoplasmic domain consists of an $\alpha/\beta/\alpha$ sandwich subdomain ($\alpha/\beta/\alpha$-SD) with a so-called divalent cation sensor (DCS) between the subunits, bearing two cation-binding sites, M1 and M2.[5,6]

The DCS is believed to function as a part of a divalent-sensing molecular switch that regulates the channel gating via the negative feedback mechanism in response to the cellular Mg^{2+} levels.[9−12] A decrease in the concentration of divalent cations and, consequently, the loss of divalent cation—protein interactions increases the flexibility of the entire protein complex, including, in particular, the CorA basic ring (residues Lys286, Lys292, Lys346−349, see Figure 1) in line with the first crystallographic structures (PDB ID: 2BBJ, 2HN2).[8,12] It has been suggested that the acidic electrostatic nature of the outer helices ($\alpha 5$ and $\alpha 6$) (Figure 1C, TM2-$\alpha 5$, $\alpha 6$ interactions)[10] of the cytoplasmic domain might be recruited to change the position of the basic ring by forming interactions with the outer TM2, which produces a gating force on the intracellular hydrophobic gate (residues Met291 and Leu294) and possibly
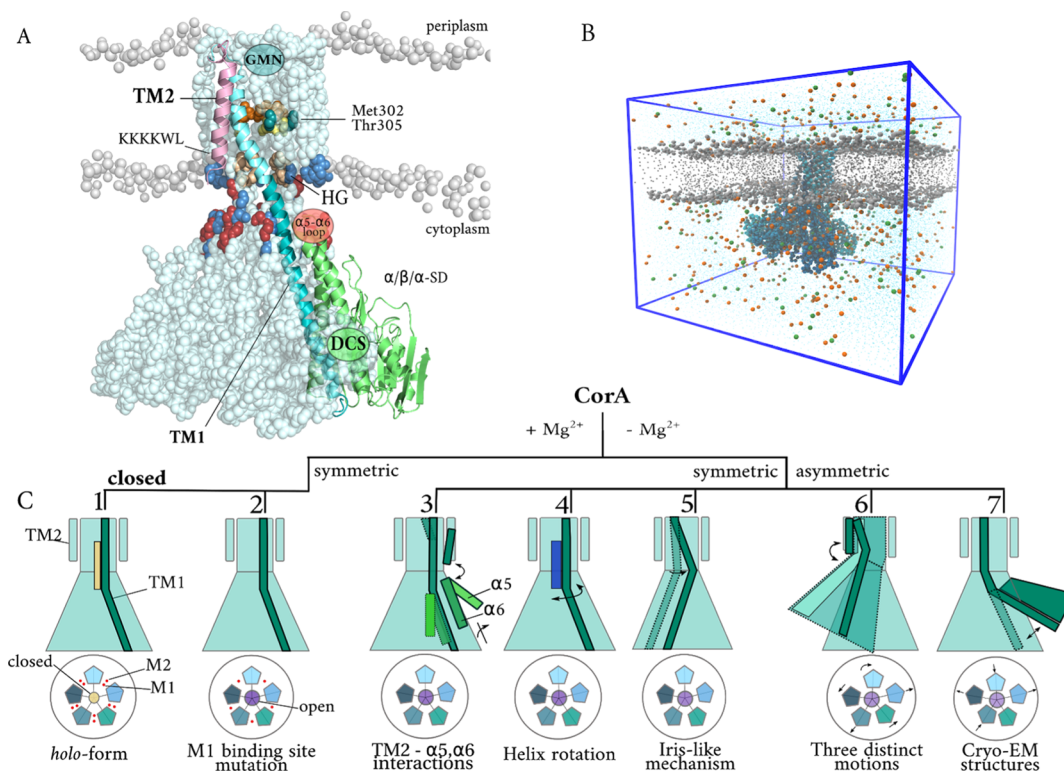
Figure 1. Overall atomistic model, CG system, and summarized scheme of known data of the gating mechanism of TmCorA. (A) Side view of the CorA AA models (AA-CorA) with basic functional details: vdW representation of wild-type CorA with one protein monomer highlighted (cartoon representation) in the closed state (PDB ID: 4I0U) with the lipid bilayer (gray; for clarity, only lipid head groups are shown). The main parts of the protein monomer are highlighted: TM1 (light cyan-transmembrane and dark cyan-cytoplasmic parts, respectively), TM2 (pink), and the cytoplasmic domain (green). Charged residues within the CorA basic and acidic rings (blue and red), the $\alpha/\beta/\alpha$-SD subdomain (funnel interior and helices), the $\alpha5-\alpha6$ loop (red circle), the divalent cation sensor (DCS, green circle), Pro303 hydrophobic belt (Met302 and Thr305), and gate (HG) are labeled. (B) Initial simulation setup of the CorA CG model (CG-CorA) into a POPE/POPG/POPC membrane (grey) with 0.15 M sodium (orange) chloride (green) solution in a water box (cyan). The blue box indicates periodic boundary conditions. (C) Schematic description of the proposed hypotheses of the CorA gating mechanism: (1) *holo* form of TmCorA in the closed state[8,12,42] and proposed gating mechanisms based on (2) M1 binding site mutations (D89K/D253K and D89R/D253R residues) in the presence of magnesium ions,[16] and (3) considerable torque along $\alpha7$ with movements of $\alpha6$ and $\alpha5$ helices,[10] (4) conversion of a closed hydrophobic gate into a an open hydrophilic one due to the $\alpha7$ helix rotation,[5] (5) iris-like mechanism,[13] (6) "three distinct motions",[7] (7) cryo-EM structures in the absence of divalent cations.[14] The circles represent the closed (yellow) and open (violet) pore of the protein. Arrows show major structural rearrangements during the gating. The major parts of the protein (TM1 and TM2) are labeled.

the Pro303 hydrophobic belt in the periplasmic region (residues Met302 and Thr305). On the other hand, according to results obtained by Chakrabarti et al. using molecular dynamics (MD) simulations, a decrease in magnesium concentration would lead to the dilation of the pore by an iris-like mechanism (Figure 1C) and subsequent wetting of the hydrophobic pore region.[13] However, in later studies, the same group has proposed a different mechanism in which channel gating is accompanied by a complex three-way movement.[7] In their work, they proposed that channel opening is caused by a combination of lateral and radial tilting of two adjacent monomers, which allows the creation of interactions between the monomers (the $\alpha5$-$\alpha6$ loop, the KKKKWL motif, and the residue Lys292) including a bell-like deflection (see Figure 1C, three distinct motions).

New details emerged with two structures of TmCorA in the proposed open state using single-particle cryo-electron micros-copy (cryo-EM).[14] It was observed that in the *apo*-form, TmCorA shows an increased asymmetrical flexibility of the cytoplasmic domains (Figure 1C). According to these new structures, the gating presumably results from the hinge-bending motion observed in the stalk helix without interaction with the transmembrane domain.[14] Such asymmetric movements of the

cytoplasmic domains were also observed recently with real-time high-speed atomic force microscopy (HS-AFM).[15] Apart from the proposed iris-like and asymmetry collapse mechanisms, the helix rotation mechanism was proposed based on mutagenesis studies and whole-cell transport assays,[5] where rotation of the $\alpha7$ helix segment replaces apolar residues with polar ones inside the pore hence allowing the ion movement (Figure 1C). Interestingly, recent crystallographic structures of one of the CorA Mg^{2+} binding site mutants (Figure 1C, M1 binding site mutation) showed a limited effect of magnesium ions on the large conformational rearrangements and transport activity.[16] The summarized picture of the proposed hypotheses to date is shown in Figure 1C. Nevertheless, none of these hypotheses revealed the actual transitions during the conversion from the closed-inactive to an open-active state and vice versa.

To address this issue, we studied the CorA gating mechanism using classical all-atom (AA) and coarse-grained (CG) MD simulations. MD simulations are a widely used tool to provide insights into the structural aspects and driving forces of membrane channel gating.[17,18] Our simulations indicate that the divalent cations are involved in the regulation of pore opening by intracellular concentration. Moreover, in the

absence of divalent ions, CorA shows the striking asymmetric mobility of the monomers and conformational rearrangements during protein gating, in agreement with the cryo-EM data, and we further validated this by site-directed mutagenesis and biochemical assays.

■ MATERIALS AND METHODS

Molecular Dynamics Simulations. We performed MD simulations of the divalent metal-ion transport proteins in aqueous salt solutions by atomistic classical (AA) and CG simulations. The TmCorA crystallographic and cryo-EM structures with the PDB ID: 4I0U (2.7 Å) and 3JCH (7.06 Å) were used as the *holo* (Mg^{2+}-bound) and the *apo*-form (Mg^{2+}-unbound) of the protein, respectively. The atomistic model of the TmCorA was modeled in Coot[19] using the previously published structures (PDB ID: 3JCH, 4I0U, 2BBH) as reference models.

All MD simulations were performed with the MD package Gromacs (version 2018).[20,21] Atomistic and CG simulations were performed with the CHARMM36[22] and Martini 3[23,24] (v3.0.b.4.28) force fields in combination with a Gō-like model,[25] respectively. Visual inspection of the trajectories was performed with VMD[37] and PyMOL (DeLano Scientific, Palo Alto, CA, USA).

AA Setup. AA MD simulations of the TmCorA models were conducted using three different model systems: (i) the crystal structure of the closed state with 13 magnesium ions, (ii) the crystal structure of the closed state with the removal of all ligands, and (iii) the cryo-EM model of the *apo*-form without magnesium ions.

The TmCorA protein structures were embedded in a hydrated 1-palmitoyl-2-oleoyl-*sn*-glycero-3-phosphocholine (POPC-PC) lipid bilayer consisting of 500 lipids and solvated with 150 mM aqueous NaCl solution. Additionally, for model system ii, the AA MD simulations have been performed in 1,2-dimyristoyl-*sn*-glycero-3-phosphocholine (DMPC) and 1-palmitoyl-2-oleoyl-*sn*-glycero-3-phosphoethanolamine (POPE-PE), 1-palmitoyl-2-oleoyl-*sn*-glycero-3-phosphoglycerol (POPG-PG), and PC (3:3:2) model membranes with the same amount of lipids and NaCl concentration.

The CHARMM36 force field was used to describe the interactions.[22] In preparing the system, the CHARMM membrane builder tool (http://www.charmm-gui.org/?doc=input/membrane.bilayer) was used. The initial box size was $13 \times 13 \times 18$ nm³. The structure was solvated using the TIP3P[26] solvent model such that every protein atom was at least 12 Å away from the side of the box. Periodic boundary conditions were employed, and the particle-mesh Ewald method[27,28] was used for treatment of long-range electrostatic interactions. The systems were optimized and equilibrated for 1 ns in the *NVT* ensemble and 10 ns in the *NPT* ensemble. The simulations were conducted at a constant semi-isotropic pressure of 1 atm and a temperature of 303.15 K using the Parrinello−Rahman barostat[29,30] and the Nosé−Hoover thermostat,[31,32] respectively. The total number of atoms in the simulation box was ∼315 000. All systems were equilibrated for 10 ns with restraints to the final simulation, which were removed in subsequent free MD simulations.

CG Setup. All CG simulations presented in our work have been performed using the Martini 3[23,24] (v3.0.b.4.28) force field with a Gō-like model, which stabilizes native interactions using additional Lennard-Jones potentials.[25,33] Lennard-Jones interactions with a dissociation energy of $\varepsilon = 12.0$ kJ/mol were used.

To build the CG CorA models, the final protein structures after AA MD simulations were used. The CG structures of the proteins were generated using the program *martinize2.py* (see https://github.com/marrink-lab/vermouth-martinize). The leap-frog propagator was employed in combination with the Verlet cutoff scheme and a buffer tolerance of 0.005 kJ/mol. Van der Waals interactions were treated using the cutoff scheme with a cutoff of 1.1 nm.[34] The temperature and pressure were controlled with a velocity-rescale thermostat (reference temperature T = 303.15 K, coupling constant τ_T = 1 ps) and a Parrinello−Rahman semi-isotropic barostat (p = 1 bar, τ_p = 12 ps, compressibility $\beta = 3 \times 10^4$ bar⁻¹), respectively.

The CG simulations of CorA have been performed in PE/PG/PC model membrane[35] with the same ratio of 3:3:2 as in our *in vitro* experiments. CorA was embedded in a PE/PG/PC bilayer in a rectangular box ($13.0 \times 13.0 \times 18.0$ nm³) using the program *insane.py*.[36] The bilayer, containing 520 lipids, was solvated in 18,457 CG water beads (representing 73,828 water molecules) and neutralized, and 0.15 M NaCl was added. Two CG simulations of 40 μs were used to investigate a series of conformational transitions during the gating of TmCorA proteins.

In the case of CorA in *apo*-form, the PE/PG/PC membrane contained, in total, 1300 lipids. It was solvated with 47,628 CG water beads (190,512 water molecules), resulting in a box of $20.0 \times 20.0 \times 20.0$ nm³. Again, 0.15 M NaCl was added to the system after neutralization. CG simulations of 30 μs were used for the comparison of conformational transitions of closed and *apo*-form TmCorA.

Analysis of Domain Orientations. Analysis of domain orientations was performed using the method of Wassenaar et al.,[38] which is based on an earlier method for decomposing MSD contributions due to domain rearrangements.[39] In short, the method determines an orientation for each domain by fitting a reference structure onto the domain structure and storing the translation vector and the rotation matrix. A single reference structure is used for similar domains. The translation vectors and rotation matrices are postprocessed to give consistent views of the orientations of domains over time and of relative orientations between domains as rotation matrices, quaternions, or Euler angles. A set of orientations can be used as a low-dimensional representation of a complex protein. To this end, the centers of mass and orientations were written as CGO objects and visualized in PyMOL (DeLano Scientific, CA, USA).

Experimental Assays. *Site-Directed Mutagenesis.* The *T. maritima* CorA gene was cloned into a pNIC28-Bsa4 vector as described previously.[4] Site-directed mutagenesis was performed using the QuikChange II Site-Directed Mutagenesis Kit (Agilent Technologies) as described by the manufacturer. All mutations were validated by DNA sequencing.

Protein Expression and Purification. Plasmids carrying the mutant CorA gene were transformed into *Escherichia coli*. The mutants and the wild-type were overexpressed in *E. coli* and purified as described previously.[4] Briefly, cells were cultivated in LB medium at 37 °C until an OD_{600} of around 0.6−0.7, and protein expression was induced by the addition of 0.2 mM IPTG for 3 h. Subsequently, cells were harvested (15 min, 7446 g, 4 °C) and washed once with 50 mM Tris−HCl, pH 8.0. Cells were resuspended in 50 mM Tris−HCl, pH 7.5, 200 μM PMSF, 1 mM $MgSO_4$, supplemented with ∼50 μg DNase per ml and lysed using a Constant Cell Disruption System (Constant Systems Ltd., UK) by 1 passage at 25 kPsi at 5 °C. Then, cell
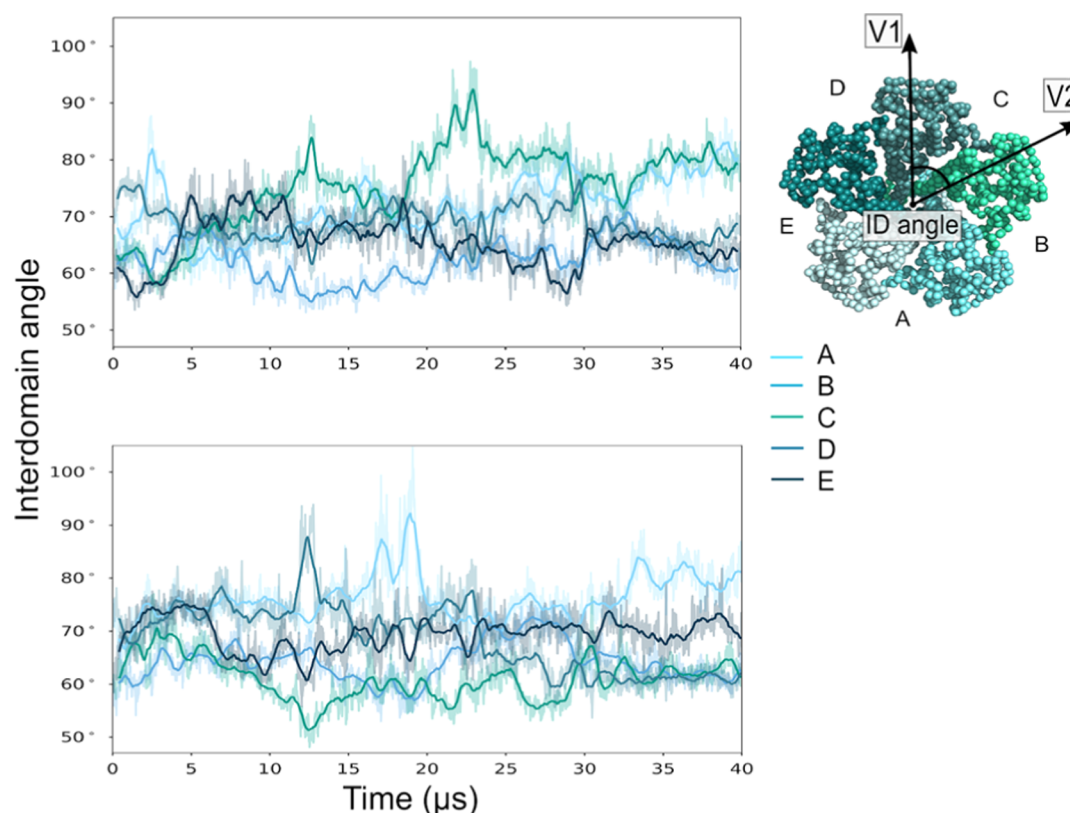
Figure 2. Asymmetry of the interdomain angle (ID angle) for all monomers of TmCorA. The graphs show the time evolution of the interdomain angle (the angle formed between the two vectors V1 and V2 connecting the center of geometry of TmCorA of α7 (residues 1−282) to the center of geometry of the full protein) for all five monomers in the closed state, for two independent simulations. Different colors represent different monomers in the system. On the right side, a schematic representation of the definition of the ID angle is shown for the closed state.

debris was removed by low-speed centrifugation (30 min, 12,074 g, 4 °C), and membrane vesicles were collected by ultracentrifugation (120 min, 193,727 g, 4 °C) and were resuspended in 50 mM Tris−HCl, pH 8.0, 200 mM NaCl, 15% glycerol. Subsequently, these membrane vesicles were frozen in liquid nitrogen and stored at −80 °C until used.

Membrane vesicles were solubilized using 1% *n*-dodecyl-β-D-maltopyranoside (DDM, Anatrace) in 50 mM Tris−HCl, pH 8.0, 250 mM NaCl, and a nonsolubilized material was removed by ultracentrifugation (30 min, 442,907 g, 4 °C). The supernatant was incubated for 1 h at 4 °C under gentle rocking with a buffer-equilibrated Ni^{2+}-Sepharose resin (column volume of 0.5 mL). This suspension was poured into a 10 mL disposable column (Bio-Rad) with the collection of the flow-through. The column material was washed with 10 mL of wash buffer [50 mM Tris−HCl, pH 8.0, 250 mM NaCl, 50 mM imidazole, 0.04% DDM]. The target protein was eluted in three fractions of 250, 750, and 500 μL of elution buffer [50 mM Tris−HCl, pH 8.0, 250 mM NaCl, 400 mM imidazole, 0.04% (w/v) DDM]. The second elution fraction was spun down on a tabletop centrifuge for 10 min at 13,000 rpm, 4 °C before purification by size-exclusion chromatography using a Superdex 200 10/300 gel filtration column (GE-Healthcare), which was pre-equilibrated with gel filtration buffer [50 mM Tris−HCl, pH 8.0, 250 mM NaCl, 0.04% (w/v) DDM]. The fractions containing the CorA were combined and used directly for proteoliposome reconstitution.

Reconstitution into Proteoliposomes and Fluorescent Transport Assay. Reconstitution in proteoliposomes and fluorescent transport assays were performed as described

previously.[4] In brief, divalent cation transport was measured with the Zn^{2+}-sensitive fluorophore FluoZin-1 (Thermo Fisher, USA) with shielding from direct light as much as possible. The fluorophore was added to a final concentration of 5 μM to the proteoliposomes with encapsulation by three freeze−thaw cycles and subsequent extrusion through a 400 nm polycarbonate filter (Avestin). The liposome suspension was run on a 2 mL Sephadex G-75 column equilibrated with ice-cold reconstitution buffer [50 mM HEPES, pH 7.5] to remove the extravesicular dye from the solution, and, subsequently, proteoliposomes were collected by ultracentrifugation (25 min, 285,775 g, 4 °C). Then, proteoliposomes were mixed with 10 μL of ice-cold reconstitution buffer per 2.5 mg of proteoliposomes [the ratio 1:250 protein/lipid (w/w)].

Transport assays were performed by the addition of 10 mM stock solution of zinc acetate $Zn(CH_3CO_2)_2$. For each measurement, 0.3 mg of proteoliposomes was mixed in 1 mL of the reconstitution buffer. A fluorescence time course was measured in a 1 mL cuvette with a stirrer (350 rpm) using an excitation wavelength of 490 nm and an emission wavelength of 525 nm. A linear regression was performed per uptake curve between 1 and 10 s after addition of divalent cations to calculate initial transport rates ($\Delta F\ s^{-1}$).

■ RESULTS

Simulations Reveal the Asymmetry of Individual CorA Monomers. To investigate the conformational transitions of TmCorA caused by a decrease in the concentration of divalent ions in the cellular environment, we performed atomistic MD simulations of TmCorA in a closed state (*holo* form) obtained
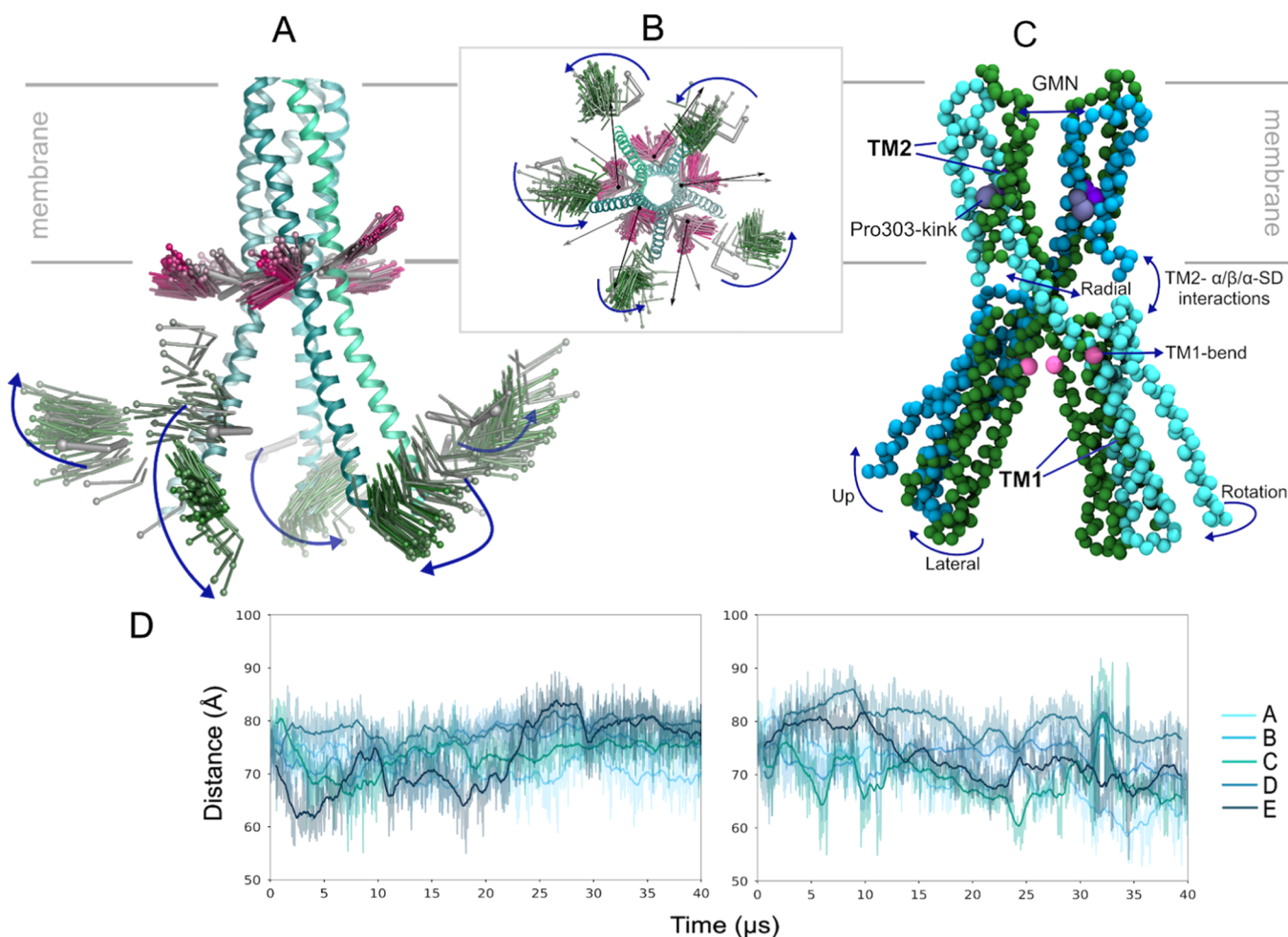
Figure 3. Analysis of TmCorA structural rearrangements during gating. (A) Side view of the TmCorA $\alpha 7$ helices together with orientational markers that summarize the set of orientations over time (gray at the start toward hot pink at the end of the simulation). In gray to green, the orientational markers of the cytoplasmic domain are shown, and the corresponding motions are highlighted with blue arrows. (B) Same as panel (A), but seen from the cytoplasmic side, with arrows added to signify the angles between the start (black) and end (gray) orientations of the $\alpha 7$ helix. (C) VdW representation of the asymmetry of the definition of motions of individual monomers of CorA, from the side view. Comparison of two backbone $\alpha 7$ helices (TM1) and TM2 of CG-CorA in the open state with the initial structure (green). The monomers are color-coded, allowing comparisons between the asymmetric motions of cytoplasmic domains at one selected MD simulation time. Arrows show major structural rearrangements during the TmCorA gating. (D) Distance profiles between the center of geometry of the N-terminal residues (1−280 residues) and the center of geometry of the membrane from two independent simulation runs. Different colors represent different monomers in the system.

from the 2.7 Å resolution X-ray structure (PDB ID: 4I0U),[5] with and without the removal of the bound Mg^{2+} ions. An additional simulation of TmCorA was performed in one of the *apo*-forms (no Mg^{2+}-bound) based on the ∼7 Å resolution cryo-EM structure (PDB ID: 3JCH).[14] For the latter, we chose a structure with the most pronounced differences relative to the available closed state structures, which supposedly represents an open TmCorA conformation.[14] Each of the channels was embedded in a POPC bilayer and simulated for 200 ns for closed states and 350 ns for the *apo*-form using the CHARMM36 force field (see Materials and Methods section and Supporting Information for details).

As anticipated, in the presence of divalent cations, the periplasmic hydrophobic belt and the intracellular hydrophobic gate (HG) in TmCorA remained dehydrated throughout the entire MD simulation of the closed state (Figure S1A). Upon removal of the bound divalent cations, we observed destabilization of the cytoplasmic domains and small asymmetric movements of the monomers, in contrast to the stable arrangement of the cytoplasmic domains in the presence of

magnesium ions (Figure S2−4). However, the expected full opening of the channel followed by its hydration, as observed previously in MD simulations of CorA channels, never occurred.[7,40] In particular, the final conformation of the TM domains still resembles that of the closed state, with the completely dehydrated region between the Pro303 hydrophobic belt (residues Met302 and Thr305) and the HG (Figure S1B). A similar retention of hydrophobic gates was also observed after MD simulation of the *apo*-form (Figure S1C).

It is possible that these atomistic simulation time spans are insufficient to follow protein conformational changes coupled to the gating of the hydrophobic pore. Furthermore, previously obtained results using AA MD simulations at different time scales[7,9,40] do not agree well with each other, and none of them can explain all other available experimental data. Therefore, to study the protein dynamics on the microsecond time scale, we performed CG MD simulations, an efficient tool to probe membrane protein gating over longer time scales at lower resolution.[41] Simulations were performed using the Martini 3 force field, starting with the structures taken from the atomistic

E
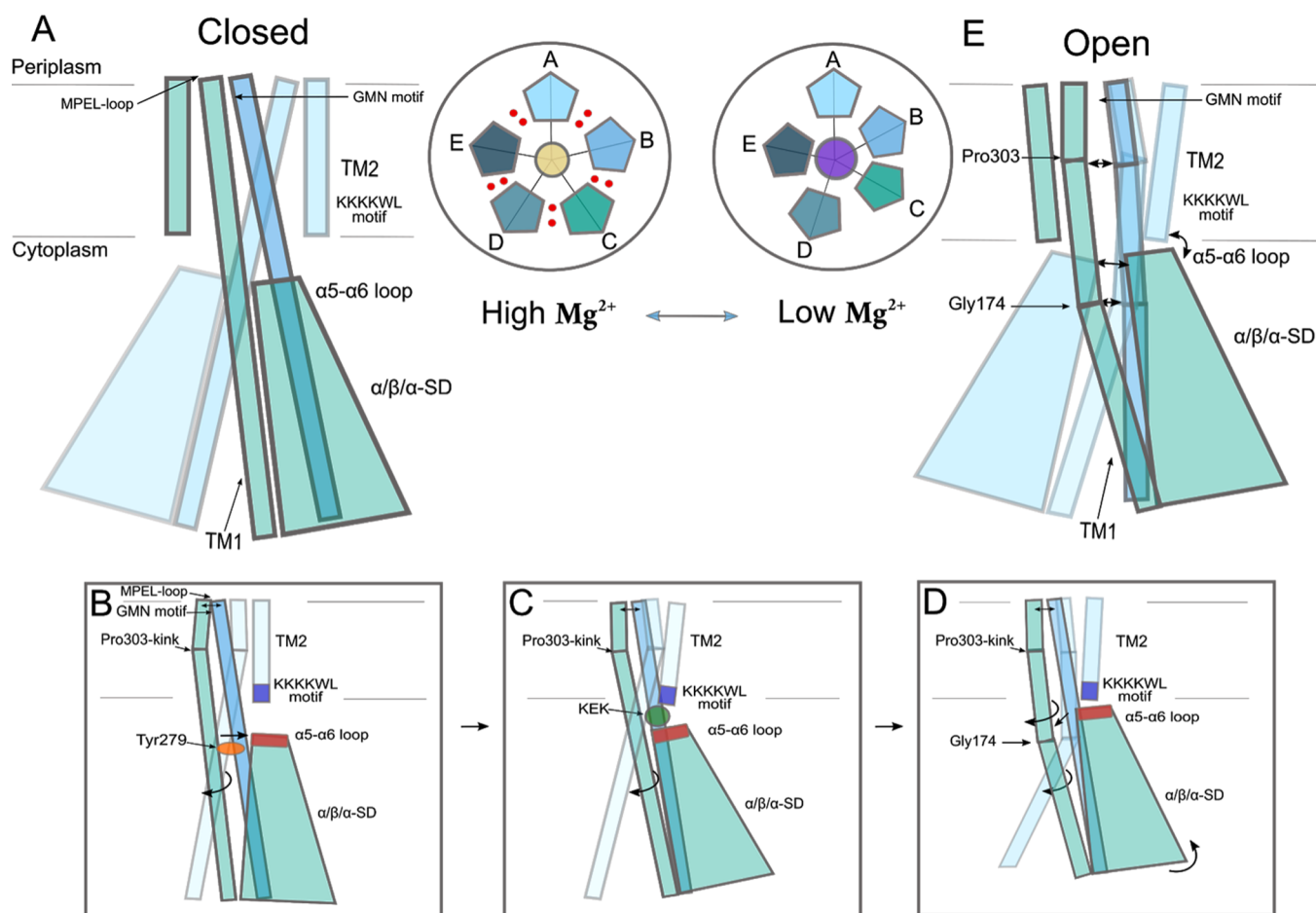
Figure 4. Schematic representation of the TmCorA gating mechanism. Structural elements are colored as in Figure 2, and only three monomers are shown for clarity. Red spheres represent the locations of cations bound in the DCS. The circles represent the closed (yellow) and open (violet) pore of the protein. A decrease in the intracellular concentration of Mg^{2+} leads to destabilization of the interaction between monomers in the closed state (A). This increases the mobility of the GMN selectivity filter (GMN motif) at the periplasmic entrance by Pro303-kink and the $\alpha/\beta/\alpha$-SD. The subsequent rotation along $\alpha7$ induces gating of the hydrophobic belt (Pro303-kink). The reorganized $\alpha5-\alpha6$ loop moves away from the main $\alpha7$ helix assisted by the hydrophobic attraction from Tyr279 (orange) (B). As a result of such conformational changes, (C) the $\alpha5-\alpha6$ loop and the KKKKWL motif move toward the monomer between them and create interactions with the polar region formed by Lys292, Glu289, and Lys286 (KEK). (D) Subsequent interaction of the $\alpha5-\alpha6$ loop and the KKKKWL motif produces a gating force on the hydrophobic gate and leads to a transition to the open state (E).

trajectories (see Materials and Methods for details). The initial system is shown in Figure 1B.

The CG simulations of the *holo*-form revealed that the removal of magnesium ions from the binding sites leads to an asymmetric conformational mobility of the CorA monomers (Figure 2, and Movie S1). To show this, we analyzed the interdomain angle of all the monomeric units that form the funnel (Figure 2). The angles in the closed starting model demonstrate high asymmetric fluctuations of the monomers already from the first microseconds of the simulations in the absence of Mg^{2+} ions, which indicates a decrease in the stabilization energy between the monomers with a subsequent increase in dynamics and conformational flexibility of the N-terminal cytoplasmic domain. Moreover, during the simulations, the protein shows conformations generally consistent with the reported asymmetric cryo-EM structures.[14]

In addition, we performed CG MD simulations of the *apo*-form. The protein exhibits similar asymmetric fluctuations as observed in the closed-state simulation (Figure S5); however, after 10 μs simulation, it forms a narrower funnel due to the rotation of the main helix as a consequence of the entire cytoplasmic domain movement, which leads to collisions of

monomers after 30 μs of MD simulation (Figure S5). This is likely the result of the decoupled movements of the transmembrane domain from the cytoplasmic domain caused by significant bends of the $\alpha7$ helices in the initial experimentally obtained structure. Such abnormal behavior may indicate that the narrowed funnel in asymmetric state II (PDB ID: 3JCH) is perhaps an artifact of vitrification.

Taken together, our MD simulations suggest that in the absence of magnesium ions, our closed state and *apo*-form CG models demonstrate strong asymmetric mobility of monomers despite further narrowing of the model funnel in the *apo*-form.

Monomer Rearrangement Enables Gate Opening. To gain more insights into the mechanism underlying the gating of TmCorA, we analyzed the structural rearrangements seen in the CG simulations in more detail, using a method for domain orientation analysis.

By monitoring the motions of $\alpha7$ helices during the closed state simulations, we observed structural changes for individual monomers as compared to the starting model (Figure 3A,B). Due to the loss of the strict symmetry in the cytoplasmic part, the $\alpha/\beta/\alpha$ sandwich subdomain forces the $\alpha7$ helix to rotate from the center of the pore, which accordingly triggers the rotation of
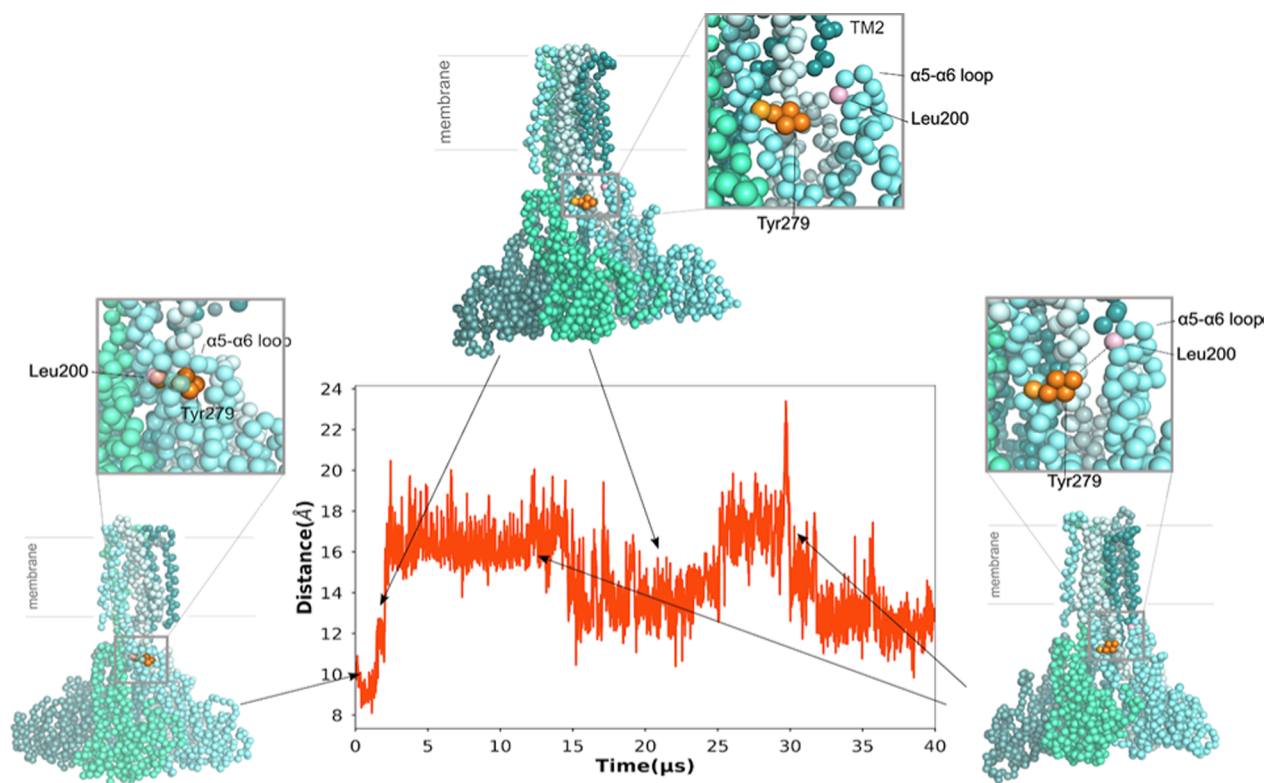
Figure 5. Role of Tyr279 in gating. Different colors represent different monomers in the system. Involvement of Tyr279 in gating the protein channel. The graph shows the time evolution of the distance between Tyr279 and the $\alpha5-\alpha6$ loop for one monomer from the closed state. With increasing destabilization of the entire cytoplasmic subdomain, the hydrophobic force created by the tyrosine residue increases the mobility of the protein elbow (the $\alpha5-\alpha6$ loop), which may impact the rate of transition of the protein from the closed to the open state. The facilitating effect of Tyr279 on the mobility of the protein elbow is observed in the first few microseconds of the transition to the open state during the destabilization of the cytoplasmic subdomain due to the absence of magnesium ions.

the entire $\alpha/\beta/\alpha$-SD domain and causes the violation of symmetry in the transmembrane part. To further explore the motions observed in the $\alpha7$ helix, we performed an analysis of the rotation of the individual helices using the motion analysis method (Figure 3B). The rotation of the helix in our simulations reached $\sim25-30°$, which is perhaps necessary to create an optimal polar surface area of the pore for the passage of the hydrated divalent cations through the channel. This is in line with the earlier experiments performed by Nordin et al.[5] who showed that the closing of the ion pathway occurs due to the $\alpha7$ helix clockwise turn with the replacement of the hydrophilic inner surface of the pore (open) with a hydrophobic one (closed). At the same time, $\alpha7$ helices from all of the monomers exhibit significant bending compared to that of the crystal structure manifesting in Pro303-kink around the periplasmic hydrophobic belt and increase in the radius of the intracellular hydrophobic gate (Met291 and Leu294) and Asn285 and Asn288 residues (Figures 3C and S6A), which are accompanied by the motions of the $\alpha/\beta/\alpha$-SD in the vertical direction and bend near Gly274 (Figure S6B).

To quantify these subsequent rearrangements of the cytoplasmic domain under the motions observed in the $\alpha7$ helix, we analyzed the temporal evolution of the monomer distances based on the center of geometry of the N-terminal residues (1-280) and membrane for 40 μs of simulation. Figure 3C,D shows an increase in mobility of $\alpha/\beta/\alpha$-SD independently for each monomer in the absence of Mg^{2+} throughout the entire trajectory. This is consistent with the previous real-time HS-AFM imaging and[15] cryo-EM structures,[14] wherein the absence

of magnesium ions caused a loss of symmetry due to the conformational changes of individual monomers with an increase in the height of protrusion which can reach ~2 nm. However, these results contrast with those reported by Kowatz and Maguire,[16] who showed limited structural changes in CorA upon mutation of the M1 binding site in the absence of magnesium ions compared to the wild type structure, where the release of ions is supposed to cause channel opening.

Proposed Asymmetric Gating Model. Based on our simulations, we propose that CorA gating occurs in several steps: first, the loss of stabilizing interactions of divalent cations on the surface of the monomers leads to an increase in dynamics and conformational flexibility of the $\alpha/\beta/\alpha$-SD. This is due to the repulsion of charges and rearrangement of the transmembrane part caused by increased MPEL-loop mobility and, subsequently, the GMN selectivity filter at the periplasmic entrance. The increased flexibility of the $\alpha/\beta/\alpha$-SD impacts the stalk $\alpha7$ helix and causes its rotation from the center of the pore (Figure 4B). This perturbs the pentameric arrangement of the GMN and the helix-breaking kink (Pro303) near Met302 and Thr305 (Figures 4 and S6A) inducing the gating of the hydrophobic belt. Such a gating mechanism is consistent with previously obtained crystallographic data on the reshaping of the selective filter to accommodate the strict coordination of magnesium ions.[6,8,10,12] The subsequent rotation of the entire $\alpha/\beta/\alpha$-SD leads to symmetry break in the transmembrane part and promotes the rearrangement of the domain (Figure 3B). The asymmetric models that we obtained from CG MD simulations are consistent with HS-AFM data.[15] The asymmetric movement
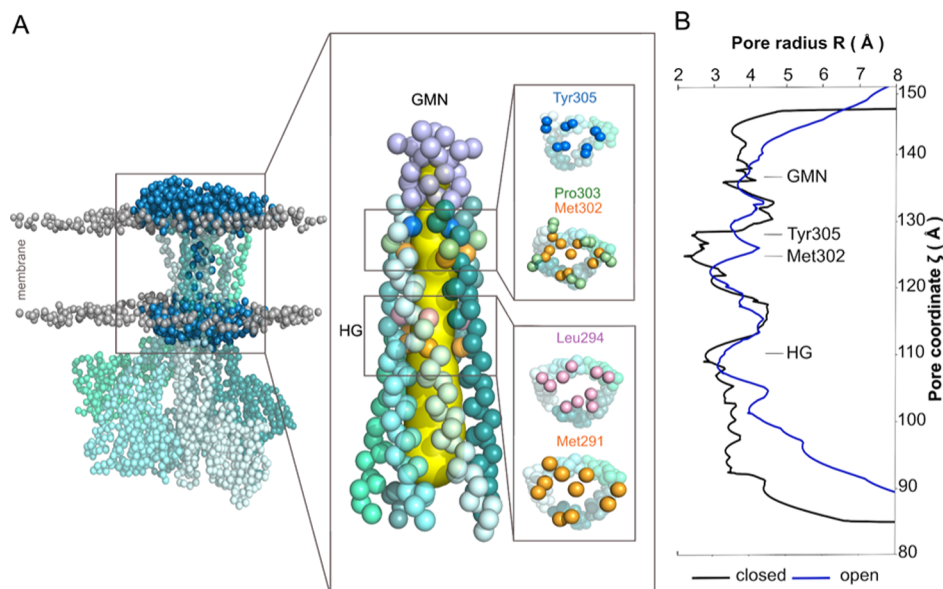
Figure 6. Model of TmCorA open channel. (A) Surface representation of the open pore diameter in the CG-TmCorA model. The water beads and the pore-lining surface are shown in dark blue and yellow, respectively. Snapshots of Met302 (orange), Met291 (orange), Pro303 (green), and Leu294 open (pink) of the open channel in the periplasmic hydrophobic belt and in the intracellular hydrophobic gate (HG) show the loss of symmetry of the transmembrane part of the channel. Pore radii were calculated with the HOLE program and the ChExVis software tool. (B) Distribution of ion channel pore radii in the CG-TmCorA model in the closed state (black) and the unbound open state (blue) in the solid line representation.

of the cytoplasmic domain is also in line with the previous structural and experimental data derived from the low resolution (~21 Å) cryo-EM structure of MjCorA obtained in low magnesium conditions and functional and biophysical (EPR, fluorescence) studies.[43] These conformational changes result in destabilization of the interaction of the acidic-rich loop region formed by $\alpha 5$ and $\alpha 6$ helices (the CorA elbow) with the $\alpha 7$ helix. The movement of the loop is assisted by the hydrophobic force created by Tyr279, which acts as a lever to push the loop away from the main $\alpha 7$ helix (Figures 4A and 5) as observed by our CG MD simulations.

The $\alpha 5-\alpha 6$ loop (Glu204, Lys205, and Glu206 (EKE)) of one monomer is displaced to the polar region formed by Lys292, Glu289, and Lys286 (KEK) on the $\alpha 7$ helix of the neighboring monomer to a distance of less than 6−7 Å forming "salt bridges" (Figures 4C and S7). This movement increases the bend and the angle of rotation of the $\alpha 7$ helix away from the permeation pathway, and subsequently, it forms a part of the gating force (Figure 4C). Our results are in agreement with the previous observations by Nordin et al., where CorA gating was shown to be achieved by rotation of the $\alpha 7$ helix, which sequentially leads to the replacement of hydrophobic residues by polar ones and thus opening the hydrophobic gates.[5] Also, the highly conserved C-terminal KKKKWL motif of TM2 moves along the main $\alpha 7$ helix neighboring monomer to KEK, forming "salt bridges" (Lys342-344). The subsequent interaction of the KKKKWL motif with the $\alpha 5-\alpha 6$ loop (Figures 4D and S7) creates an additional pulling force on the $\alpha 7$ helix from the channel central axis, which creates a polar environment with the size suitable for the passage of the partially hydrated divalent ions through the channel (Figure 6).

Site-Directed Mutagenesis Experiments Validate Simulations. To validate our hypothesis and shift the protein toward a closed state, we performed site-directed mutagenesis. On the basis of our MD simulations results, we hypothesized that the replacement of Tyr279 could affect the transport activity

of the protein. We aimed to check the importance of the interactions between the $\alpha 5-\alpha 6$ loop of $\alpha / \beta / \alpha$-SD and the $\alpha 7$ stalk helix by replacing the Tyr279 to valine (Y279V), phenylalanine (Y279F), and glutamate (Y279E) (Table S1). We obtained similar protein expression levels during the large-scale purification of the membrane fractions for all the mutants comparable with the wild-type TmCorA (see Figure S8 for the gel−filtration profiles and SDS-PAGE/WB). To investigate mutant transport activity, we performed a fluorescent transport assay by using the Zn^{2+}-sensitive fluorophore FluoZin-1 as it was shown before as a suitable probe to study *in vitro* transport in the CorA family of proteins.[4]

Mutation of Y279F removed the hydroxyl group from the aromatic ring and reduced the Zn^{2+} transport to approximately 50% of the wild type (Figure 7). This decrease in transport activity is probably the result of a stronger interaction of the charged residues of the $\alpha 5-\alpha 6$ loop with the $\alpha 7$ helix, which prevents the formation of new interactions with the positively charged end of TM2 (interactions between residues Lys347−349 and Glu201, Glu204) and due to the increased surface hydrophobicity.

To further test the importance of pocket hydrophobicity, we made the Y279V mutant hence replacing the aromatic ring with a hydrophobic aliphatic side chain. This mutation retained about 60% transport activity of the wild-type TmCorA (Figure 7). Interestingly, with the introduction of the negative charge (Y279E mutation), the inhibitory effect on the TmCorA Zn^{2+} transport was almost equivalent to that of the Y279F mutation. Apparently, negatively charged glutamate creates new interactions with positively charged amino acid residues of the $\alpha 5-\alpha 6$ loop, such as Arg202 and Lys205, which also can limit the mobility of the loop.

■ DISCUSSION

TmCorA is an important model protein for studying the transport mechanism of essential biological divalent metal
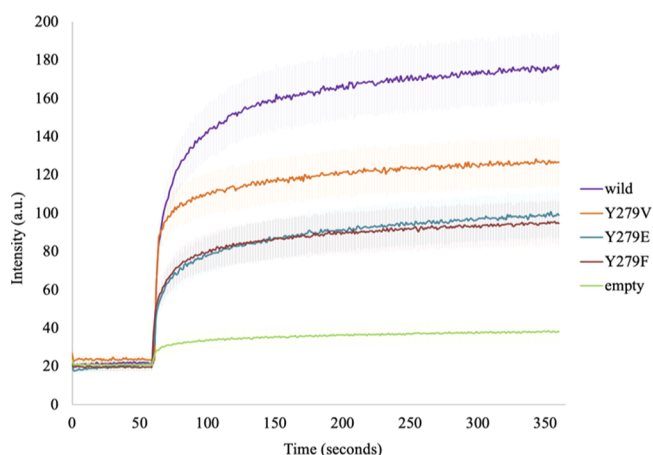
Figure 7. Zn^{2+} transport by TmCorA reconstituted into proteoliposomes. The transport activity of TmCorA with Y279V (orange), Y279E (cyan), or Y279F (red) mutant was assayed by the fluorophore of FluoZin-1 dye trapped inside the proteoliposomes. The wild-type TmCorA (wild, amethyst) and the empty CorA-less liposomes (empty, green) with 20 μM Zn^{2+} were used as positive and negative controls, respectively. The experiments were performed in three technical replicates of independent batches of proteoliposomes.

cations in prokaryotes and their eukaryotic homologues. However, despite the fairly complete characterization by a wide range of structural, biochemical, and functional approaches, the exact transition of a protein from a closed state to a functionally active state in TmCorA is still unclear.

Based on the obtained results in this work and the data published previously, we propose an updated TmCorA gating mechanism (Figure 4). In general, the removal of divalent metal cations from the protein, in particular, from the acidic inter-SD interface, triggers relaxation and destabilization of interactions due to repulsion of charges. This in turn initiates the rearrangement of the whole N-terminal $\alpha/\beta/\alpha$ sandwich subdomain and subsequently causes rotation of the stalk α7 helix from the center of the pore with breaking of symmetry. Furthermore, our CG MD simulations revealed increased mobility and flexibility of the acidic-rich α5−α6 loop with its further displacement to the polar region on the α7 helix and the formation of interaction with the TM2 helix through one monomer as a result of increased mobility of the entire cytoplasmic subdomain and bends of the main helix (Gly274). Together, these movements would have the combined effect of opening the intracellular hydrophobic gate located at Leu294 and Met291 creating a pore with the size suitable for the passage of the partially hydrated divalent ions through the channel.

Additionally, it is interesting to note that Tyr279 of the main α7 helix, due to its hydrophobicity and size, might facilitate the process of detachment of the α5−α6 loop from the main α7 helix and enhance its mobility. Although the introduced mutations did not show a complete inhibitory effect on the transport activity of the TmCorA, given the obtained MD results and the evolutionary conservation of this tyrosine, at least in Subgroup A for CorA,[44] this residue might play an important role in protein transition from the closed to the open state and back.

Our results contradict the hypotheses of the symmetric domain rearrangement. Chakrabarti[13] and others[9] proposed an iris-like mechanism according to which channel watering occurs due to the symmetric expansion of the hydrophobic pore with an increase of the lateral tilt of α7 helices. Specifically, the idea of

expanding the diameter of the pathway for the passage of the partially hydrated divalent cation is consistent with our results, but in our case, this is primarily due to the rotation and flexibility of the α7 helix with the subsequent movement of the cytoplasmic subdomain. This is similar to the proposition made by Nordin et al., where the polar permeation path is created by the rotation of the α7 helix followed by the replacement of hydrophobic residues with polar ones.[5] This rotation most probably corresponds to our proposed helical turn due to the interaction of the TM2 with the α5−α6 loop.

Other studies have also pointed out the importance of the interaction of the transmembrane and the cytoplasmic domains, which may play a major role in TmCorA gating;[10,12] for example, Payandeh et al.[10] proposed that the loss of cation binding at the DCS site causes a dramatic structural rearrangement of the cytoplasmic subdomain and subsequent swivel of the α6 helix with the movement of the α5 helix through the twisting of the α7 helix, which creates an additional force on the hydrophobic gate.

Other asymmetrical structural rearrangements and TM-SD interactions were observed in AA MD simulations in the absence of the Mg^{2+}[7], namely, the formation of salt bridges between the α5−α6 loop and the C-terminal KKKKWL motif of the adjacent monomer as a result of the strong bending of the stalk α7 helix at the residue Gly274 and the subsequent bell-bending motion of the entire cytoplasmic domain due to combination of lateral and radial tilts and rotation along the channel axis of monomers. However, in our simulations, we observed the interaction of the α5−α6 loop with the KKKKWL motif of TM2 of the same monomer, which could give more freedom for rotation and increase the diameter of the periplasmic pore.

Interestingly, structures of mutants from the divalent cation sensor have been recently reported[16] and the claim has been made that metal binding sites do not play a role in the formation of a closed state, implying that TmCorA is able to maintain its pentameric state in the absence of divalent ions. However, given a rather low resolution of these mutant structures, the actual presence of the magnesium in M2 sites, and the availability of numerous experimental data,[8−11,15] such an assumption cannot be correct.

We note that in our CG simulation of the *apo*-form after 10 μs of increased mobility of monomers, the structure demonstrates a strong narrowing of the funnel, which has not been observed in simulations of closed-state models. As we can assume, it could have happened due to the high mobility of the cytoplasmic domain due to the strong bend of the α7 helix without affecting the transmembrane domain. Such a kink at the residue Gly274 (and Asp277) was also seen in low-resolution cryo-EM structures[14] of TmCorA in the absence of magnesium with retainment of an approximate five-fold symmetry of the transmembrane domain, that is, in contradiction with our simulation results of the open-II structure (PDB ID: 3JCH).

These highly dynamic conformational changes of individual monomers in our simulations are consistent with recent studies on protein structural rearrangements caused by the decrease in magnesium concentration in real-time[15] and as seen in asymmetric cryo-EM structures.[14] However, it is important to emphasize that the resolution of these cryo-EM structures and HS-AFM data is limited and cannot give a precise picture of the ensemble of multiple intermediate structures and detailed changes in the conformation of the hydrophobic pore region at the molecular level.

Importantly, such asymmetrical conformational states are also observed in completely unrelated proteins, such as a

mitochondrial Hsp90 chaperon Trap1[45,46] and 5-HT$_{3A}$ serotonin receptor,[47] indicating that the asymmetry might be a more common phenomenon.

Taken together, our results show that the divalent metal cations are involved in the regulation of pore opening, where the intracellular concentration is sensed via cytoplasmic binding sites and where ion-unbinding energies are used to power the transition from the closed state to the open state. We also propose a gating mechanism that consists of an ensemble of several asymmetric movements including interactions between the TM2 helix and $\alpha 5-\alpha 6$ loops in SD. Our results reconcile with the existing gating hypotheses of the CorA proteins, providing a molecular picture of the mechanism of transport of divalent cations via this protein.

■ ASSOCIATED CONTENT

ⓈⒾ Supporting Information

The Supporting Information is available free of charge at https://pubs.acs.org/doi/10.1021/acs.jcim.1c00261.

> Properties of AA MD of TmCorA; rmsd analysis of the AA MD simulations; rmsd values of backbone atoms for all monomers; root-mean-square fluctuation analysis of the AA MD simulations; CG MD simulations of *apo*-form CorA; profiles of local bends of TmCorA; TM2-$\alpha 5$-$\alpha 6$ loop interactions; and quality control of the mutations produced (PDF)

> Asymmetric transition of TmCorA monomers from the closed to an open state during the CG MD simulation (MP4)

■ AUTHOR INFORMATION

Corresponding Authors

Siewert J. Marrink − *Groningen Institute for Biomolecular Sciences and Biotechnology, University of Groningen, 9747AG Groningen, The Netherlands;* ⓞ orcid.org/0000-0001-8423-5277; Phone: +31 50 36 34457; Email: s.j.marrink@rug.nl

Albert Guskov − *Groningen Institute for Biomolecular Sciences and Biotechnology, University of Groningen, 9747AG Groningen, The Netherlands;* ⓞ orcid.org/0000-0003-2340-2216; Phone: +31 50 36 34391; Email: a.guskov@rug.nl

Authors

Mariia Nemchinova − *Groningen Institute for Biomolecular Sciences and Biotechnology, University of Groningen, 9747AG Groningen, The Netherlands*

Josef Melcr − *Groningen Institute for Biomolecular Sciences and Biotechnology, University of Groningen, 9747AG Groningen, The Netherlands*

Tsjerk A. Wassenaar − *Groningen Institute for Biomolecular Sciences and Biotechnology, University of Groningen, 9747AG Groningen, The Netherlands*

Complete contact information is available at:
https://pubs.acs.org/10.1021/acs.jcim.1c00261

Author Contributions

M.N. designed the research with suggestions from S.J.M., A.G., and J.M., and M.N. performed the simulations; all authors analyzed the data. The paper was written by M.N., A.G, S.J.M., J.M., and T.A.W with contributions of all authors. All authors have given approval to the final version of the paper.

■ ABBREVIATIONS

TmCorA, CorA protein from the thermophilic bacterium *Thermotoga maritima*; GMN, glycine−methionine−asparagine selectivity filter; TM1, $\alpha 7$ helix; TM2, outer transmembrane helix; $\alpha/\beta/\alpha$-SD, $\alpha/\beta/\alpha$ sandwich subdomain; DCS, divalent cation sensor; MD, molecular dynamics; cryo-EM, cryo-electron microscopy; HS-AFM, real-time high-speed atomic force microscopy; AA, all-atom; CG, coarse-grained; HG, hydrophobic gate; AA-CorA, CorA AA model; CG-CorA, CorA CG model; ID angle, interdomain angle; SEC, size-exclusion chromatography; LJ, Lennard-Jones; PME, particle mesh Ewald; DDM, *n*-dodecyl-β-D-maltopyranoside

■ REFERENCES

(1) Aryal, P.; Sansom, M. S. P.; Tucker, S. J. Hydrophobic Gating in Ion Channels. *J. Mol. Biol.* **2015**, *427*, 121−130.

(2) Knoop, V.; Groth-Malonek, M.; Gebert, M.; Eifler, K.; Weyand, K. Transport of Magnesium and Other Divalent Cations: Evolution of the 2-TM-GxN Proteins in the MIT Superfamily. *Mol. Genet. Genomics* **2005**, *274*, 205−216.

(3) Schindl, R.; Weghuber, J.; Romanin, C.; Schweyen, R. J. Mrs2p Forms a High Conductance Mg^{2+} Selective Channel in Mitochondria. *Biophys. J.* **2007**, *93*, 3872−3883.

(4) Stetsenko, A.; Guskov, A. Cation Permeability in CorA Family of Proteins. *Sci. Rep.* **2020**, *10*, 840.

(5) Nordin, N.; Guskov, A.; Phua, T.; Sahaf, N.; Xia, Y.; Lu, S.; Eshaghi, H.; Eshaghi, S. Exploring the Structure and Function of Thermotoga Maritima CorA Reveals the Mechanism of Gating and Ion Selectivity in Co^{2+}/Mg^{2+} Transport. *Biochem. J.* **2013**, *451*, 365−374.

(6) Eshaghi, S.; Niegowski, D.; Kohl, A.; Martinez Molina, D.; Lesley, S. A.; Nordlund, P. Crystal Structure of a Divalent Metal Ion Transporter CorA at 2.9 Angstrom Resolution. *Science* **2006**, *313*, 354−357.

(7) Pfoh, R.; Li, A.; Chakrabarti, N.; Payandeh, J.; Pomès, R.; Pai, E. F. Structural Asymmetry in the Magnesium Channel CorA Points to Sequential Allosteric Regulation. *Proc. Natl. Acad. Sci. U.S.A.* **2012**, *109*, 18809−18814.

(8) Payandeh, J.; Pai, E. F. A structural basis for Mg2+ homeostasis and the CorA translocation cycle. *EMBO J.* **2006**, *25*, 3762−3773.

(9) Dalmas, O.; Sompornpisut, P.; Bezanilla, F.; Perozo, E. Molecular Mechanism of Mg^{2+}-Dependent Gating in CorA. *Nat. Commun.* **2014**, *5*, 3590.

(10) Payandeh, J.; Li, C.; Ramjeesingh, M.; Poduch, E.; Bear, C. E.; Pai, E. F. Probing Structure-Function Relationships and Gating Mechanisms in the CorA Mg^{2+} Transport System. *J. Biol. Chem.* **2008**, *283*, 11721−11733.

(11) Palombo, I.; Daley, D. O.; Rapp, M. The Periplasmic Loop Provides Stability to the Open State of the CorA Magnesium Channel. *J. Biol. Chem.* **2012**, *287*, 27547−27555.

(12) Lunin, V. V.; Dobrovetsky, E.; Khutoreskaya, G.; Zhang, R.; Joachimiak, A.; Doyle, D. A.; Bochkarev, A.; Maguire, M. E.; Edwards, A. M.; Koth, C. M. Crystal Structure of the CorA Mg²⁺ Transporter. *Nature* **2006**, *440*, 833−837.

(13) Chakrabarti, N.; Neale, C.; Payandeh, J.; Pai, E. F.; Pomès, R. An Iris-like Mechanism of Pore Dilation in the CorA Magnesium Transport System. *Biophys. J.* **2010**, *98*, 784−792.

(14) Matthies, D.; Dalmas, O.; Borgnia, M. J.; Dominik, P. K.; Merk, A.; Rao, P.; Reddy, B. G.; Islam, S.; Bartesaghi, A.; Perozo, E.; et al. Cryo-EM Structures of the Magnesium Channel CorA Reveal Symmetry Break upon Gating. *Cell* **2016**, *164*, 747−756.

(15) Rangl, M.; Schmandt, N.; Perozo, E.; Scheuring, S. Real Time Dynamics of Gating-Related Conformational Changes in CorA. *Elife* **2019**, *8*, No. e47322.

(16) Kowatz, T.; Maguire, M. E. Loss of Cytosolic Mg2 Binding Sites in the Thermotoga Maritima CorA Mg²⁺ Channel Is Not Sufficient for Channel Opening. *Biochim. Biophys. Acta, Gen. Subj.* **2019**, *1863*, 25−30.

(17) Flood, E.; Boiteux, C.; Lev, B.; Vorobyov, I.; Allen, T. W. Atomistic Simulations of Membrane Ion Channel Conduction, Gating, and Modulation. *Chem. Rev.* **2019**, *119*, 7737−7832.

(18) Zhekova, H. R.; Ngo, V.; da Silva, M. C.; Salahub, D.; Noskov, S. Selective Ion Binding and Transport by Membrane Proteins − A Computational Perspective. *Coord. Chem. Rev.* **2017**, *345*, 108−136.

(19) Emsley, P.; Lohkamp, B.; Scott, W. G.; Cowtan, K. Features and Development of Coot. *Acta Crystallogr., Sect. D: Biol. Crystallogr.* **2010**, *66*, 486−501.

(20) Pronk, S.; Páll, S.; Schulz, R.; Larsson, P.; Bjelkmar, P.; Apostolov, R.; Shirts, M. R.; Smith, J. C.; Kasson, P. M.; van der Spoel, D.; et al. GROMACS 4.5: A High-Throughput and Highly Parallel Open Source Molecular Simulation Toolkit. *Bioinformatics* **2013**, *29*, 845−854.

(21) Abraham, M. J.; Murtola, T.; Schulz, R.; Páll, S.; Smith, J. C.; Hess, B.; Lindahl, E. GROMACS: High Performance Molecular Simulations through Multi-Level Parallelism from Laptops to Supercomputers. *SoftwareX* **2015**, *1−2*, 19−25.

(22) Huang, J.; MacKerell, A. D., Jr. CHARMM36 All-Atom Additive Protein Force Field: Validation Based on Comparison to NMR Data. *J. Comput. Chem.* **2013**, *34*, 2135−2145.

(23) Marrink, S. J.; Tieleman, D. P. Perspective on the Martini Model. *Chem. Soc. Rev.* **2013**, *42*, 6801−6822.

(24) Souza, P. C. T.; Alessandri, R.; Barnoud, J.; Thallmair, S.; Faustino, I.; Grünewald, F.; Patmanidis, I.; Abdizadeh, H.; Bruininks, B. M. H.; Wassenaar, T. A.; et al. Martini 3: A General Purpose Force Field for Coarse-Grained Molecular Dynamics. *Nat. Methods* **2021**, *18*, 382−388.

(25) Poma, A. B.; Cieplak, M.; Theodorakis, P. E. Combining the MARTINI and Structure-Based Coarse-Grained Approaches for the Molecular Dynamics Studies of Conformational Transitions in Proteins. *J. Chem. Theory Comput.* **2017**, *13*, 1366−1374.

(26) Jorgensen, W. L.; Chandrasekhar, J.; Madura, J. D.; Impey, R. W.; Klein, M. L. Comparison of Simple Potential Functions for Simulating Liquid Water. *J. Chem. Phys.* **1983**, *79*, 926−935.

(27) Darden, T.; York, D.; Pedersen, L. Particle Mesh Ewald: AnN·log(N) Method for Ewald Sums in Large Systems. *J. Chem. Phys.* **1993**, *98*, 10089−10092.

(28) Essmann, U.; Perera, L.; Berkowitz, M. L.; Darden, T.; Lee, H.; Pedersen, L. G. A Smooth Particle Mesh Ewald Method. *J. Chem. Phys.* **1995**, *103*, 8577−8593.

(29) Parrinello, M.; Rahman, A. Polymorphic Transitions in Single Crystals: A New Molecular Dynamics Method. *J. Appl. Phys.* **1981**, *52*, 7182−7190.

(30) Nosé, S.; Klein, M. L. Constant Pressure Molecular Dynamics for Molecular Systems. *Mol. Phys.* **1983**, *50*, 1055−1076.

(31) Nosé, S. A Unified Formulation of the Constant Temperature Molecular Dynamics Methods. *J. Chem. Phys.* **1984**, *81*, 511−519.

(32) Hoover, W. G. Canonical Dynamics: Equilibrium Phase-Space Distributions. *Phys. Rev. A* **1985**, *31*, 1695−1697.

(33) Souza, P. C. T.; Thallmair, S.; Marrink, S. J.; Mera-Adasme, R. An Allosteric Pathway in Copper, Zinc Superoxide Dismutase Unravels the Molecular Mechanism of the G93A Amyotrophic Lateral Sclerosis-Linked Mutation. *J. Phys. Chem. Lett.* **2019**, *10*, 7740−7744.

(34) de Jong, D. H.; Baoukina, S.; Ingólfsson, H. I.; Marrink, S. J. Martini Straight: Boosting Performance Using a Shorter Cutoff and GPUs. *Comput. Phys. Commun.* **2016**, *199*, 1−7.

(35) Marrink, S. J.; de Vries, A. H.; Mark, A. E. Coarse Grained Model for Semiquantitative Lipid Simulations. *J. Phys. Chem. B* **2004**, *108*, 750−760.

(36) Wassenaar, T. A.; Ingólfsson, H. I.; Böckmann, R. A.; Tieleman, D. P.; Marrink, S. J. Computational Lipidomics with Insane: A Versatile Tool for Generating Custom Membranes for Molecular Simulations. *J. Chem. Theory Comput.* **2015**, *11*, 2144−2155.

(37) Humphrey, W.; Dalke, A.; Schulten, K. VMD: Visual Molecular Dynamics. *J. Mol. Graphics* **1996**, *14*, 33−38.

(38) Wassenaar, T. A.; Pluhackova, K.; Moussatova, A.; Sengupta, D.; Marrink, S. J.; Tieleman, D. P.; Böckmann, R. A. High-Throughput Simulations of Dimer and Trimer Assembly of Membrane Proteins. The DAFT Approach. *J. Chem. Theory Comput.* **2015**, *11*, 2278−2291.

(39) Wassenaar, T. A. Molecular Dynamics of Sense and Sensibility in Processing and Analysis of Data. PhD Thesis, University of Groningen, Groningen, 2006.

(40) Neale, C.; Chakrabarti, N.; Pomorski, P.; Pai, E. F.; Pomès, R. Hydrophobic Gating of Ion Permeation in Magnesium Channel CorA. *PLoS Comput. Biol.* **2015**, *11*, No. e1004303.

(41) Melo, M. N.; Arnarez, C.; Sikkema, H.; Kumar, N.; Walko, M.; Berendsen, H. J. C.; Kocer, A.; Marrink, S. J.; Ingólfsson, H. I. High-Throughput Simulations Reveal Membrane-Mediated Effects of Alcohols on MscL Gating. *J. Am. Chem. Soc.* **2017**, *139*, 2664−2671.

(42) Guskov, A.; Nordin, N.; Reynaud, A.; Engman, H.; Lundbäck, A.-K.; Jong, A. J. O.; Cornvik, T.; Phua, T.; Eshaghi, S. Structural Insights into the Mechanisms of Mg²⁺ Uptake, Transport, and Gating by CorA. *Proc. Natl. Acad. Sci. U.S.A.* **2012**, *109*, 18459−18464.

(43) Cleverley, R. M.; Kean, J.; Shintre, C. A.; Baldock, C.; Derrick, J. P.; Ford, R. C.; Prince, S. M. The Cryo-EM Structure of the CorA Channel from Methanocaldococcus Jannaschii in Low Magnesium Conditions. *Biochim. Biophys. Acta* **2015**, *1848*, 2206−2215.

(44) Niegowski, D.; Eshaghi, S. The CorA Family: Structure and Function Revisited. *Cell. Mol. Life Sci.* **2007**, *64*, 2564−2574.

(45) Moroni, E.; Agard, D. A.; Colombo, G. The Structural Asymmetry of Mitochondrial Hsp90 (Trap1) Determines Fine Tuning of Functional Dynamics. *J. Chem. Theory Comput.* **2018**, *14*, 1033−1044.

(46) Elnatan, D.; Betegon, M.; Liu, Y.; Ramelot, T.; Kennedy, M. A.; Agard, D. A. Symmetry Broken and Rebroken during the ATP Hydrolysis Cycle of the Mitochondrial Hsp90 TRAP1. *Elife* **2017**, *6*, No. e25235.

(47) Zhang, Y.; Dijkman, P. M.; Zou, R.; Zandl-Lang, M.; Sanchez, R. M.; Eckhardt-Strelau, L.; Köfeler, H.; Vogel, H.; Yuan, S.; Kudryashev, M. Asymmetric Opening of the Homopentameric 5-HT Serotonin Receptor in Lipid Bilayers. *Nat. Commun.* **2021**, *12*, 1074.